





Dynamic modeling and identification of a reluctance synchronous machine parameters

Łukasz J. NIEWIARA¹ *, Michał GIERCZYŃSKI² , Tomasz TARCZEWSKI¹ ,
and Lech M. GRZESIAK² 

¹ Institute of Engineering and Technology, Nicolaus Copernicus University in Torun, ul. Wilenska 7, 87-100 Torun, Poland

² Institute of Control and Industrial Electronics, Warsaw University of Technology, ul. Koszykowa 75, 00-662 Warsaw, Poland

Abstract. This article discusses an identification and modeling approach of a reluctance synchronous motor (RSM) based on the running rotor technique. The applied flux linkage approximation functions reflect the self-saturation and cross-saturation effects, and the applied mathematical model is continuous and differentiable. The proper design of the experiment is discussed, and relevant recommendations are made to ensure the mitigation of procedural mistakes in the experiments. A detailed analysis of the impact of configuration faults on the obtained experimental data is provided, considering distortions in the obtained flux linkage and inductance surfaces. Considering the achieved model accuracy, a novel model evaluation considering the achieved model accuracy technique based on transient current response is proposed.

Keywords: reluctance synchronous motor; electrical circuit modeling; parameter identification; dynamic modeling.

1. INTRODUCTION

In recent years, a trend for developing electric motor-based drive systems with reduced content of permanent magnets (PMs) is observed [1, 2]. This leads to rare-earth-elements-free (REE-free) constructions caused by the economic inconvenience of still growing REE-PMs prices on the market [1, 2]. Compact design, high efficiency, and reliability are crucial since the machines may be applied by various industrial branches. Among several candidates, the reluctance synchronous motors (RSMs) fulfill the requirements defined [2]. Its manufacturing cost is about 15÷20% lower, and the efficiency is up to 4% better than that of a squirrel cage induction motor (SCIM) [1]. Thus, the RSM drives become popular in such industrial applications as pumps, fans, compressors [3], lift traction [4], and finally, electric vehicles (EVs) [5]. The proper selection of a drive system is application-driven; among several criteria like dynamics, robustness, and efficiency, another criterion becomes important, i.e., acoustic noise generation [6], especially in the EVs area.

Since the operation principle of RSMs is based on the magnetic reluctance phenomenon, no eddy currents are produced for rotor excitation, in contrast to SCIMs [3, 7]. Thus, a specific salient pole rotor construction is necessary, which ensures energy-effective operation [1, 7]. The high saliency ratio is achieved using a transverse laminated anisotropic-rotor (TLA) [1]. A non-uniform distribution of axial flux barriers across the rotor achieves magnetic anisotropy. Therefore, the

non-linear saturated characteristic of the magnetic circuit determines the operating principle of these types of motors. Since the magnetic saturation effect is present, the relation between inductance components versus the stator current components becomes strongly non-linear and cross-coupled [7]. This impacts the machine electrical and mechanical properties, resulting in complex modeling approaches for the electrical circuit and torque characteristics. Thus, the precise modeling of RSMs is challenging.

Developing advanced and precise mathematical models for RSM-based drive systems can offer several benefits, like [2, 8–12]:

- 1) the optimal torque versus current or voltage characteristics may be distinguished using the offline calculation for a wide motor operation range;
- 2) power maximizing control characteristics according to angular velocity can be determined;
- 3) the performance of different machine models or types may be compared without a need for a detailed FEMM analysis;
- 4) the development and synthesis of advanced control systems will be accelerated by applying a numerical simulation model.

Thus, modern control engineering applies the numerical modeling approach as an integral element for designing advanced and high-performing systems. Therefore, obtaining a reliable and accurate mathematical description becomes a crucial issue.

In the scientific literature, numerous papers discuss the identification and modeling of RSMs. The existing approaches for identification techniques can be divided into two groups, i.e., standstill [10, 13, 14] and running rotor approach [8, 15–17]. In [2], it has been indicated that the moving rotor approach is more accurate and less prone to errors since the current and ap-

*e-mail: lukniewiara@umk.pl

Manuscript submitted 2024-02-21, revised 2024-06-07, initially accepted for publication 2024-06-08, published in September 2024.

plied voltages are averaged for one or several rotor revolutions. It results in some robustness against periodic voltage distortions, mechanical factors (shaft misalignment and eccentricity), and harmonics. Therefore, the identification procedure discussed in this study is based on a running rotor approach. Nevertheless, the accuracy of the identification experiment may suffer from numerous factors, leading to identification errors and uncertainties, e.g., experimental setup configuration, data acquisition, processing, and machine stator heating. Moreover, most scientific papers do not discuss the factors mentioned above in detail. Only a few papers discuss the impact of machine heating up (resistance variations) and voltage distortions (dead-time phenomenon) and try to cope with them [8]. This can be recognized as a potential gap in the scientific knowledge. Moreover, the literature review revealed that the model quality evaluation is mainly based on the expected shape of the flux surface [2], FEMM model results [13, 17], or response for a closed control loop [10]. Therefore, the design of a reliable evaluation technique for the model accuracy and convergence with the machine under test will be a straightforward extension of the existing knowledge.

This study tries to fill the recognized gaps in the scientific literature. More specifically, it defines recommendations for the configuration of the experimental setup. It investigates the impact of position sensor misalignment, electrical angle lag, and the impact of stator resistance variations on the estimated flux linkage and inductance surfaces. In addition, a simple and reliable model validation procedure based on an open-loop current transient response is proposed. The study will provide a broader perspective on the factors affecting the estimated flux linkage and inductance surfaces. This will help to recognize anomalies in the raw experimental data, give feedback to potential readers on how to interpret the nonphysical results, and help identify the source of potential troubles during the identification experiment.

This paper is an extension of the conference paper [18], in which the modeling and identification approach were discussed. The introduced upgrades are focused on the impact of resistance mismatch on the processed data, obtained flux and inductance surfaces, and improper experimental setup configuration. The original paper has been reorganized and enhanced by additional data and discussion. Section 2 describes the assumed current-vector-based state-space mathematical model of the RSM. The data acquisition, processing, and model fitting for obtained flux linkage maps are discussed in Section 3, emphasizing hardware limitations and configuration issues. The machine under consideration and investigation is a 3GAL092513-ASB motor manufactured by ABB. The flux linkage and static inductance components are provided, and the approximation results using the developed model are considered. Section 4 considers the impact of resistance mismatch on the processed data for several scenarios. The transient current response of the developed model is compared to experimental data and discussed in detail in Section 5. Further, Section 6 considers the impact on the estimated experimental data caused by an improper configuration of the experimental setup. The last part concludes the paper.

2. THE MATHEMATICAL MODEL OF THE ELECTRICAL CIRCUIT

Since the discussed machine is REE-free, it contains no magnets in its rotor structure (Fig. 1). Thus, the iron magnetic saturation phenomenon is revealed, and the cross-saturation effect occurs for this type of construction.

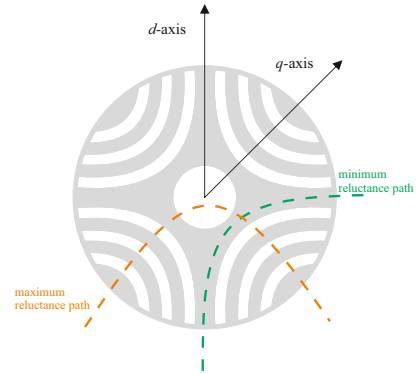


Fig. 1. Cross-section of the flux-barrier-type TLA rotor of the tested motor

The mathematical model of the reluctance synchronous machine may be expressed in the flux-voltage form using the following equations [9, 10, 13, 19]:

$$\frac{d}{dt}\psi_d(t) = u_d(t) - R_s i_d(t) + p_p \omega_m(t) \psi_q(t), \quad (1)$$

$$\frac{d}{dt}\psi_q(t) = u_q(t) - R_s i_q(t) - p_p \omega_m(t) \psi_d(t), \quad (2)$$

where: $\psi_d(t)$, $\psi_q(t)$, $u_d(t)$, $u_q(t)$, $i_d(t)$, $i_q(t)$ – the flux linkage, voltage, and current components in direct and quadrature axes, respectively, R_s – resistance of stator windings, $\omega_m(t)$ – angular velocity of the motor shaft, p_p – number of pole pairs.

Electric machine modeling requires a model where the current vector components are assumed to be state variables. Therefore, the flux model in (1) and (2) should be transformed into a current-based model assuming the following dependencies [9, 10]:

$$\psi_d(t) = L_d(i_d, i_q) i_d(t), \quad (3)$$

$$\psi_q(t) = L_q(i_d, i_q) i_q(t), \quad (4)$$

where: $L_d(i_d, i_q)$, $L_q(i_d, i_q)$ – static direct and quadrature inductance components, respectively.

Taking into account equations (3) and (4) in (1) and (2), the time derivatives of flux linkages become the following form:

$$\begin{aligned} \frac{d}{dt}\psi_d(t) &= L_d(i_d, i_q) \frac{d}{dt} i_d(t) \\ &+ i_d(t) \left[\frac{\partial L_d(i_d, i_q)}{\partial i_d} \frac{di_d}{dt} + \frac{\partial L_d(i_d, i_q)}{\partial i_q} \frac{di_q}{dt} \right], \end{aligned} \quad (5)$$

$$\frac{d}{dt}\psi_q(t) = L_q(i_d, i_q) \frac{d}{dt}i_q(t) + i_q(t) \left[\frac{\partial L_q(i_d, i_q)}{\partial i_d} \frac{di_d}{dt} + \frac{\partial L_q(i_d, i_q)}{\partial i_q} \frac{di_q}{dt} \right]. \quad (6)$$

Finally, the electrical circuit can be approximated by the following mathematical model:

$$\frac{d}{dt}\mathbf{x}(t) = \mathbf{L}_s^{-1}\mathbf{A}\mathbf{x}(t) + \mathbf{L}_s^{-1}\mathbf{u}(t), \quad (7)$$

with:

$$\mathbf{L}_s = \begin{bmatrix} L_{dd} & L_{dq} \\ L_{qd} & L_{qq} \end{bmatrix}, \quad \mathbf{x}(t) = [i_d(t), i_q(t)]^T, \\ \mathbf{u}(t) = [u_d(t), u_q(t)]^T, \\ \mathbf{A} = \begin{bmatrix} -R_s & p_p\omega_m(t)L_q(i_d, i_q) \\ -p_p\omega_m(t)L_d(i_d, i_q) & -R_s \end{bmatrix},$$

where:

$$L_{dd} = L_d(i_d, i_q) + i_d(t) \frac{\partial L_d(i_d, i_q)}{\partial i_d}, \\ L_{dq} = i_d(t) \frac{\partial L_d(i_d, i_q)}{\partial i_q}, \\ L_{qd} = i_q(t) \frac{\partial L_q(i_d, i_q)}{\partial i_d}, \\ L_{qq} = L_q(i_d, i_q) + i_q(t) \frac{\partial L_q(i_d, i_q)}{\partial i_q},$$

L_{dd} and L_{qq} – differential direct and quadrature self-axis inductance components, respectively, L_{dq} and L_{qd} – differential cross-coupling inductance components.

It can be seen that the model provided in (7) describes a non-stationary and cross-coupled plant. Moreover, the magnetic saturation phenomenon results in the machine non-linear flux linkage characteristics [10, 18]. It should be noted that the iron saturation phenomenon results in inductance variations caused by the stator current. The increase of both the direct- and quadrature current components causes a decrease of the direct- and quadrature inductance components [9, 10]. The impact of self-axis current is dominant for the self-axis inductance variations. Simultaneously increasing the orthogonal-axis current component causes a less significant inductance drop and is related to the cross-saturation phenomenon [9, 10].

3. DATA ACQUISITION, PROCESSING AND MODEL FITTING

3.1. Experimental setup configuration

The experimental tests and data capturing were realized using an experimental bed shown in Fig. 2. The setup consists of an own-designed prototype drive system with the investigated reluctance machine and an auxiliary drive system with a squirrel cage induction motor – ABB 3GAA092214-ASE three-phase motor controlled by ABB ACS880-01-04A0 inverter. The core of the

identified motor drive system is a Kinetis MKV58F1M0VLL24 microcontroller with a 240 MHz core clock. The stator current measurements are realized using LEM LTS-15-NP current transducers. The rotor mechanical angle is measured using an absolute angular sensor Sick Hiperface SFS60. The identified machine is an ABB 3GAL092513-ASB three-phase RSM. A time interval of 100 μ s was set for the data acquisition and execution of the controller subroutine, which corresponds to a frequency of 10 kHz.

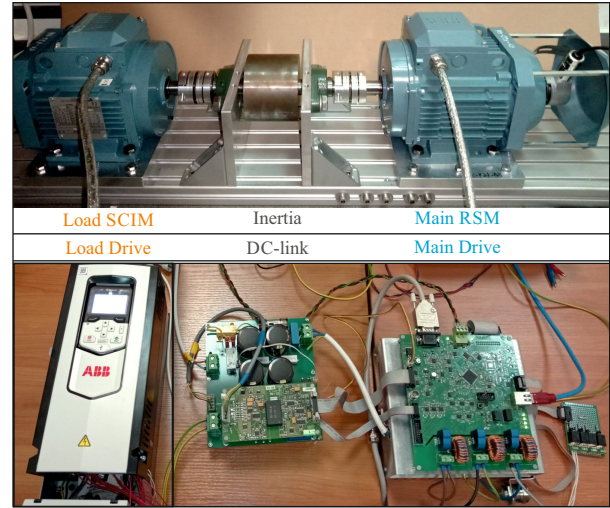


Fig. 2. The experimental bed applied for experimental tests and data capturing

The motor electrical circuit parameters were identified based on a running-rotor identification approach [8, 15]. The overall block diagram of the system is shown in Fig. 3. It consists of two drives, where the shafts of both machines are coupled via additional inertia. The experimental data were recorded for the generator operation mode of the identified machine due to the hardware limitations of the experimental bed. Thus, the applied angular velocity had an opposite sign to the applied torque in each of the four identified quadrants. Drive with SCIM was applied to maintain constant angular velocity, whereas the identified RSM operated in a current control mode. The data acquisition procedure was discussed in detail in [18]. The identified motor operated in current control mode and rotated with a fixed angular velocity set by the auxiliary SCIM. The phase current

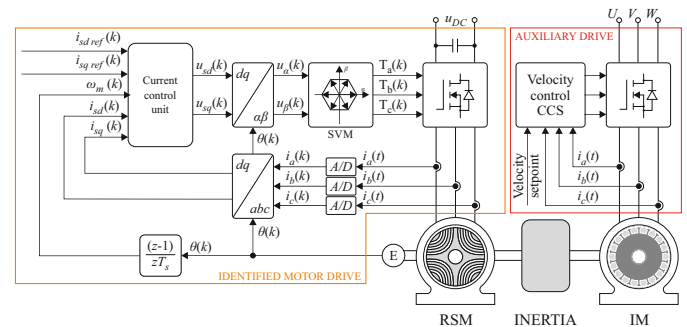


Fig. 3. Block diagram of the experimental setup for parameter identification

response was recorded for consecutive direct axis current steps for a fixed value of quadrature axis current. The range of the direct and quadrature current components was $(-5; 5)$ A with a grain of 0.25 A.

Since a discrete control system with pulse-width modulation (PWM) technique was applied, the time relation between data acquisition, controller output calculation, and control signal update was crucial for adequately measuring the average phase current value and using a synchronized average value of the phase voltage. A detailed timing diagram is shown in Fig. 4. The sampling is executed in the mid-point of the generated rectangular voltage signal, where the control signal is updated if the counter value reaches its maximum value. Since a one-sample time delay occurred in the applied system, the electrical angle applied for inverse Park transformation (dq to $\alpha\beta$) was predicted to ensure a proper generation of the desired average voltage.

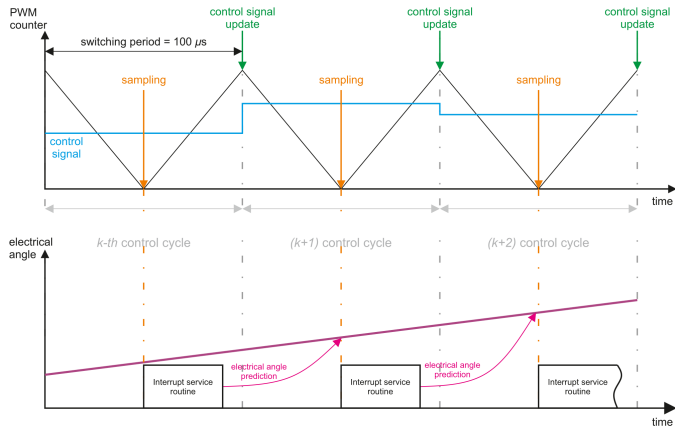


Fig. 4. Timing diagram for the applied control system for identification procedure

Reliable measurements require a proper configuration of the experimental bed to avoid data corruption caused by, e.g., power stage voltage distortions, the phase shift in measured currents, or electrical angle misalignment. The mentioned factors impact the accuracy of recorded data, so it is essential to mitigate their effect on the data acquisition. It can be reached by applying (i) dead-time effect compensation, (ii) a sufficient bandwidth of measurement paths, and (iii) proper identification of encoder alignment [18, 20]. The first two issues can be easily resolved by proper hardware design. The electrical angle alignment requires more attention since an identification procedure should be applied. In [18], this issue has been described in detail. The most important steps are as follows: (i) apply consecutive voltage vectors defined in the alpha-beta plane for the forward and backward rotation, (ii) record the measured electrical angle, (iii) calculate the mean value of the angle offset for each applied vector for the forward and reverse rotation, (iv) calculate the mean angle offset using the previously calculated points. The obtained results are shown in Fig 5. The angle offset alignment is commonly limited to measuring the offset for one single voltage vector. According to Fig. 5, this approach will lead to a significant error in electrical angle alignment. The

impact of encoder misalignment was discussed with an example in [18].

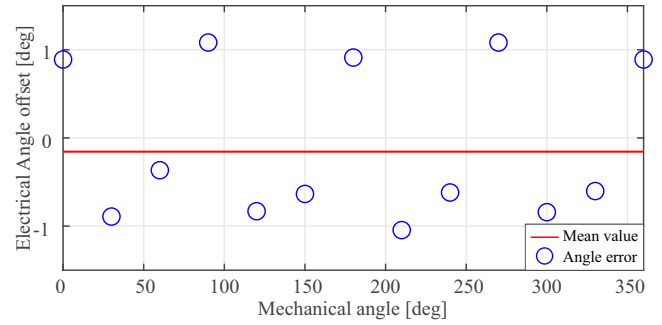


Fig. 5. The obtained electrical angle error distribution

3.2. Flux linkage estimation based on raw experimental data

The recorded signals, i.e., current and voltage components and angular velocity, were preprocessed, and their mean values in steady-state were extracted for all reference operating points. Accordingly, the model described in equations (1) and (2) can be transformed into the following static model since the time derivatives become zero in steady-state:

$$\bar{\psi}_d(\bar{i}_d, \bar{i}_q) = \frac{\bar{u}_q - R_s \bar{i}_q}{p_p \bar{\omega}_m}, \quad (8)$$

$$\bar{\psi}_q(\bar{i}_d, \bar{i}_q) = -\frac{\bar{u}_d - R_s \bar{i}_d}{p_p \bar{\omega}_m}, \quad (9)$$

where: \bar{Y}_x – the mean value of the signal Y_x at steady state, where x represents the direct (d) or quadrature (q) axis, and Y represents the flux linkage (ψ), voltage (u) or current (i), respectively.

The applied voltage is not measured directly; thus, the estimated value is calculated based on the control voltage components given by the current control unit. Therefore, it becomes essential to compensate for the non-linear phenomena present in the inverter powers stage [8].

After the data processing and calculation of the estimated flux values for each operating point of the drive, the map of direct- and quadrature flux linkage components is obtained.

Applying the described methodology and data-capturing issues, the flux linkage maps versus motor current can be estimated using equations (8) and (9) [18]. The obtained flux linkage maps are presented in Fig. 6. The saturation effect is present in the self-axis for both flux linkage components. A clearly non-linear dependence is observed. Moreover, the cross-coupling effect is present, too, revealing the flux linkage drop while the absolute value of the orthogonal current component increases. The surface analysis indicates that the obtained characteristics align with theoretical expectations. Thus, the estimated flux characteristics are initially considered proper.

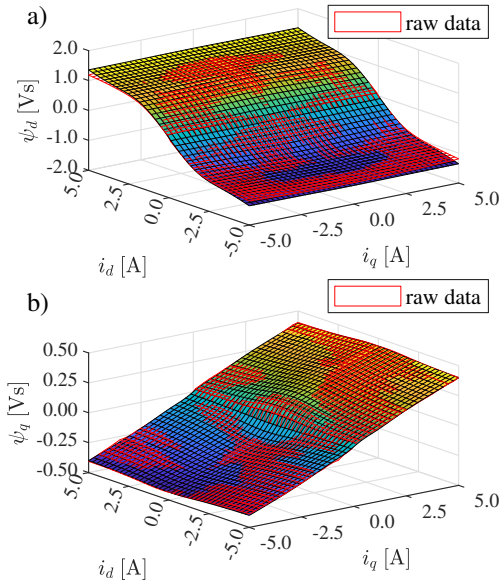


Fig. 6. Flux linkage fitting results, raw experimental data and its approximation by the assumed mathematical model, (a) direct axis, (b) quadrature axis

3.3. Mathematical model for flux linkage approximation

The developed model for dynamic modeling should ensure a proper convergence with the estimated flux linkage map, be able to reflect the self-saturation, cross-coupling, and cross-saturation effects, and according to equation (7) it has to be differentiable. The selected approximation functions should be able to reconstruct the mentioned phenomena properly [18]. It should be noted that the inverter-fed machine enables the direct measure of the machine phase currents, where the applied voltage has to be estimated based on the applied control signals. Thus, the flux linkage can not be directly measured and must also be estimated. Similarly, the static and differential inductance components must be calculated based on the assumed flux linkage model. Considering all the mentioned requirements and limitations, the following flux linkage approximation functions were selected [10, 18]:

$$\hat{\psi}_d(i_d, i_q) = W_{d0}i_d - W_{d1}W_{dq}i_d, \quad (10)$$

$$\hat{\psi}_q(i_d, i_q) = W_{q0}i_q - W_{q1}W_{qd}i_q, \quad (11)$$

with:

$$W_{d0} = A_{d0} + B_{d0}/(i_d^4 + C_{d0}i_d^2 + D_{d0}),$$

$$W_{d1} = B_{d1}/(i_d^4 + C_{d1}i_d^2 + D_{d1}),$$

$$W_{q0} = A_{q0} + B_{q0}/(i_q^4 + C_{q0}i_q^2 + D_{q0}),$$

$$W_{q1} = B_{q1}/(i_q^4 + C_{q1}i_q^2 + D_{q1}),$$

$$W_{dq} = A_{dq} - B_{dq}/(C_{dq}i_q^2 + 1),$$

$$W_{qd} = A_{qd} - B_{qd}/(C_{qd}i_d^2 + 1),$$

where: $\hat{\psi}_d(i_d, i_q)$, $\hat{\psi}_q(i_d, i_q)$ – flux linkage approximation functions, in direct and quadrature axis, respectively, A_{d0} , B_{d0} , C_{d0} , D_{d0} , B_{d1} , C_{d1} , D_{d1} , A_{dq} , B_{dq} , C_{dq} – constants in $\hat{\psi}_d(i_d, i_q)$,

A_{q0} , B_{q0} , C_{q0} , D_{q0} , B_{q1} , C_{q1} , D_{q1} , A_{qd} , B_{qd} , C_{qd} – constants in $\hat{\psi}_q(i_d, i_q)$. The first terms, i.e., W_{d0} and W_{q0} in (10) and (11) are related to self-axis flux linkage component. It represents the flux linkage variations related to the self-axis current component, while the orthogonal component equals zero. The second term, i.e., $W_{d1}W_{dq}$ and $W_{q1}W_{qd}$ in (10) and (11) are related to the cross-coupling phenomenon, i.e., to the interference with the orthogonal and self-axis current components on the flux linkage. Thus, the discussed approximation functions consider both the self-inductance and cross-coupling phenomena.

Table 1

Identification results of equations (10) and (11)

A_{d0}	B_{d0}	C_{d0}	D_{d0}	B_{d1}	C_{d1}	D_{d1}
0.2448	-202.26	4.39	33.32	1.956	4.611	35.17
A_{dq}	B_{dq}	C_{dq}	–	A_{qd}	B_{qd}	C_{qd}
-114.5	1.982	0.118	–	-108.05	117.57	0.1416
A_{q0}	B_{q0}	C_{q0}	D_{q0}	B_{q1}	C_{q1}	D_{q1}
0.0721	-1.911	6.78	10.45	101.26	50 571	59 619

Note that the provided mathematical model in (10) and (11) are continuous even functions, differentiable for current components in the range $i_{d|q} \in (-\infty; +\infty)$. This feature enables the application of these functions to calculate the static and differential inductance components. After applying the derivative operation (5) and (6) in (10) and (11) the following mathematical formulas are determined:

$$\hat{L}_{dd}(i_d, i_q) = W_{d0} - W_{d1}W_{dq} + i_d(W_{d0}' - W_{d1}'W_{dq}), \quad (12)$$

$$\hat{L}_{dq}(i_d, i_q) = -i_d(W_{d1}'W_{dq}'), \quad (13)$$

$$\hat{L}_{qd}(i_d, i_q) = -i_q(W_{q1}'W_{qd}'), \quad (14)$$

$$\hat{L}_{qq}(i_d, i_q) = W_{q0} - W_{q1}W_{qd} + i_q(W_{q0}' - W_{q1}'W_{qd}), \quad (15)$$

with:

$$W_{d0}' = -B_{d0}(4i_d^3 + 2C_{d0}i_d)/(i_d^4 + C_{d0}i_d^2 + D_{d0})^2,$$

$$W_{d1}' = -B_{d1}(4i_d^3 + 2C_{d1}i_d)/(i_d^4 + C_{d1}i_d^2 + D_{d1})^2,$$

$$W_{dq}' = 2B_{dq}C_{dq}i_q/(C_{dq}i_q^2 + 1)^2,$$

$$W_{qd}' = 2B_{qd}C_{qd}i_d/(C_{qd}i_d^2 + 1)^2,$$

$$W_{q0}' = -B_{q0}(4i_q^3 + 2C_{q0}i_q)/(i_q^4 + C_{q0}i_q^2 + D_{q0})^2,$$

$$W_{q1}' = -B_{q1}(4i_q^3 + 2C_{q1}i_q)/(i_q^4 + C_{q1}i_q^2 + D_{q1})^2,$$

where: $\hat{L}_{dd}(i_d, i_q)$, $\hat{L}_{dq}(i_d, i_q)$, $\hat{L}_{qd}(i_d, i_q)$, $\hat{L}_{qq}(i_d, i_q)$ – differential inductance approximation functions for electrical circuit modeling.

Data fitting is essential for obtaining the gain coefficients for the assumed approximation functions. The model coefficients are given in equations (10) and (11) were determined using Matlab *curve fitting toolbox* based on the estimated flux surfaces. The estimation results are shown in Fig. 6 and Fig. 7.

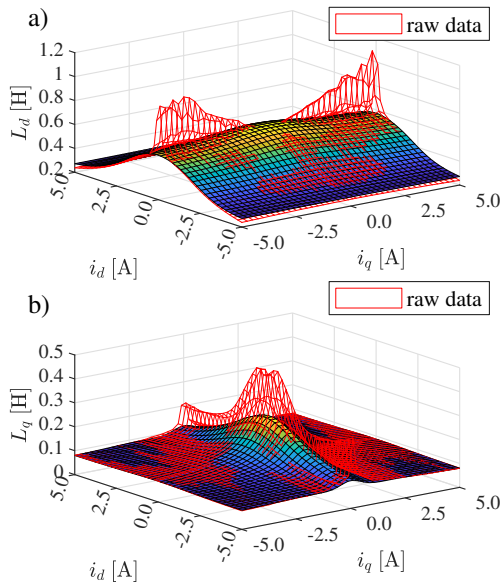


Fig. 7. Static direct and quadrature inductance components, raw experimental data and its approximation by the assumed mathematical model, (a) direct axis, (b) quadrature axis

A relatively good fit is obtained for the flux linkage components. The results correspond to the estimated surfaces obtained from the experimental data. For the inductance components, a significant distortion is present along the orthogonal current axis at low current values of the self-axis current. This is observed for a narrow current range, i.e., $\in (-0.25; 0.25)$ A. The raw data for the discussed narrow range discloses the increase of the inductance corresponding to the orthogonal current component – a nonphysical behavior contradicting the phenomenon of cross-saturation. The mentioned effect is present mainly on the direct axis and partially on the quadrature axis. Moreover, the raw data highlights a relatively high peak value, corresponding to the relatively rapid growth of the quadrature flux linkage component before saturation. The applied approximation functions cannot match the steep saturation in the quadrature axis for the provided raw data. Nevertheless, the comparison of transient response conducted in the next section reveals a good convergence of the dynamic properties of the developed model and the plant. Thus, the Authors decided to investigate the origins of the observed distortions.

3.4. Fitting results and its accuracy

According to equations (3) and (4), the inductance components can be calculated based on the estimated flux linkage components and the measured current components. Mainly, the most significant deviations are observed along the orthogonal axis at low current values in the self-axis. The observed effect is inherent in the applied estimation technique. According to equations (8) and (9), the estimation is based on the cross-coupling phenomenon. Hence, the estimated value of the flux linkage for a given operating point is calculated using the orthogonal axis voltage and current. The low self-axis current produces relatively low flux in its original axis; therefore, the measurement errors and machine parameter uncertainties will cause relatively

large estimation errors. The larger current produces higher Joule losses in the machine phase coils, which heats the stator. In consequence, the resistance of the copper wires increases. Another issue is related to the overestimating of the resistance. It is usually caused by the two-wire measurement of resistance, which is vulnerable to measurement errors related to terminal connections and auxiliary wirings. Since the resistance is not directly measured during the experiments, the actual value is not considered in the estimation formulas. This reveals the sensitivity of the applied identification approach for resistance mismatch discussed in the scientific literature [8]. Moreover, estimation errors accumulate due to current measurement errors and unmodeled voltage deviations of the inverter power stage, especially for low self-axis current components. As a result, distortions in raw data are observed. Note that the relatively long time data recording procedure causes the heating of the machine under-test. These issues, i.e., experiment duration and machine heating, are recognized as practical limitations of the applied identification technique.

The earlier-mentioned issues can be recognized as a drawback of the investigated identification procedure since they affect the accuracy of the estimated flux surfaces. It should be noted that the model-based surfaces are smoother since the fitting process is based on minimizing the root mean square error. Therefore, the influence of the estimation error is limited, but a reliable model is still obtained, which is investigated later in this paper. Hence, the Authors decided to investigate the impact of under- and overestimation of the stator resistance on the obtained raw data.

4. IMPACT OF RESISTANCE MISMATCH ON THE MODEL

4.1. Flux and inductance surface distortion for a constant resistance error

Since the assumed identification approach is related to the estimation of flux surfaces according to equations (8) and (9), it is vulnerable to any significant resistance error. It can be easily seen that if higher current is applied, the corresponding flux distortion will increase. This phenomenon is crucial in the applied identification procedure, and the knowledge about its impact on the processed numerical data can help recognize identification issues. Thus, the Authors decided to investigate the impact of resistance mismatch on the modeling and identification process for an RSM. It has been assumed that the observed distortions and anomalies are caused mainly by resistance variations (under- or overestimation) during the data-collecting procedure. A non-constant distribution of the stator resistance is assumed and simulated based on the developed model of the investigated machine. The procedure was as follows: (i) It has been assumed that the idealized model corresponds to the tested machine characteristics and becomes the simulation reference. This was chosen due to the properties of the selected approximation functions that reflect the physical phenomena present in the machine; (ii) The equations (8) and (9) with the fitted approximation functions (10) and (11) will be applied for the calculation of the machine voltage components for the simulated resistance mismatch or distribution; (iii) For the calculated voltages the flux

linkage components were again calculated using equations (8) and (9) but using the nominal (constant) value of the resistance. Thanks to this approach, it is possible to simulate what the raw identification data would look like (for a machine with characteristics such as those from the fitted model) if the value of the machine resistance would differ from that assumed during the identification.

The first investigated case represents the machine 4% higher resistance value than the value applied for estimation. A significant inductance drop is observed for the direct inductance component along the orthogonal current component axis for low self-axis current component values. It can be indicated that the observed distortion does not match the results obtained in the raw experimental data (Fig. 7a). An opposite behavior is observed for the quadrature inductance component, i.e., its value increases for the direct current component for low values of the quadrature component. This is observed in the raw experimental data, too (Fig. 7b).

Since the assumed value of the stator resistance can be overestimated due to the limited accuracy of the two-wire measurement approach, this case has also been investigated. Figure 9 provides the simulation results for flux linkage estimation by applying a higher resistance value than in the machine model (the machine has a 4% lower resistance). In this case, the constant error increases the direct axis inductance component for low values of the self-axis current component along the orthogonal component. This effect corresponds to the raw experimental data. For the quadrature axis, the observed effect is the opposite; the

inductance value drops more rapidly for the increasing value of the direct current component.

The simulated data for the manipulated resistance values indicate that the results obtained in the experimental raw data (Fig. 7) combine over- and underestimation of the tested machine resistance. Thus, the Authors investigated one more case with a non-constant resistance distribution. This assumption was concluded since both types of resistance errors may have appeared – overestimating the nominal value of the resistance caused by the two-wire measurement technique and later underestimating related to the heating of the stator caused by the Joule losses in the machine windings. It should be pointed out that experimental data collection was realized in series for a fixed value of quadrature current component and variable direct current component, starting from zero current once positive current values are applied and then applying negative current values. Therefore, it can be assumed that the resistance value was overestimated for low current values around zero and underestimated for higher values. Moreover, the rise in resistance was related mainly to the increasing direct current component. According to the assumption, the direct inductance component will increase for low self-axis current for the area with overestimated resistance, whereas distortion of the quadrature inductance component is negligible. Later, with the stator heating, the winding resistance will increase and finally reach a higher value than assumed – and the underestimating region is reached. A behavior similar to Fig. 8 would appear in this case. If those two effects overlap, they should have similar characteristics to the raw experimental data

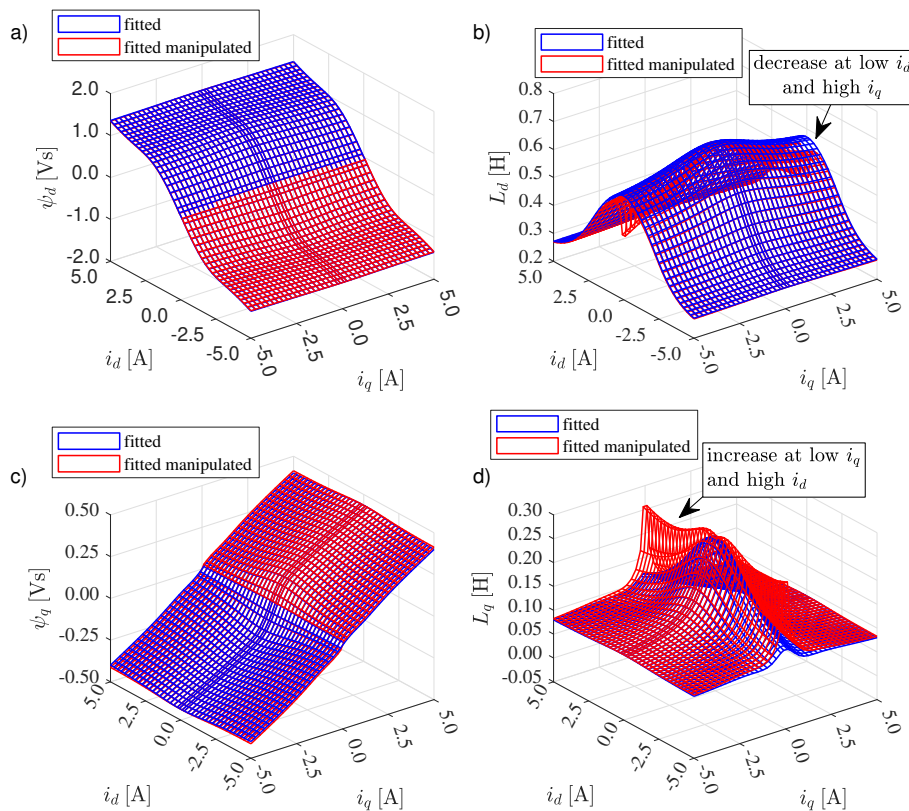


Fig. 8. The comparison of applied reference flux- and inductance model with a 4% higher resistance in the machine model (a) direct axis flux linkage, (b) direct axis static inductance, (c) quadrature axis flux linkage, (d) quadrature axis static inductance

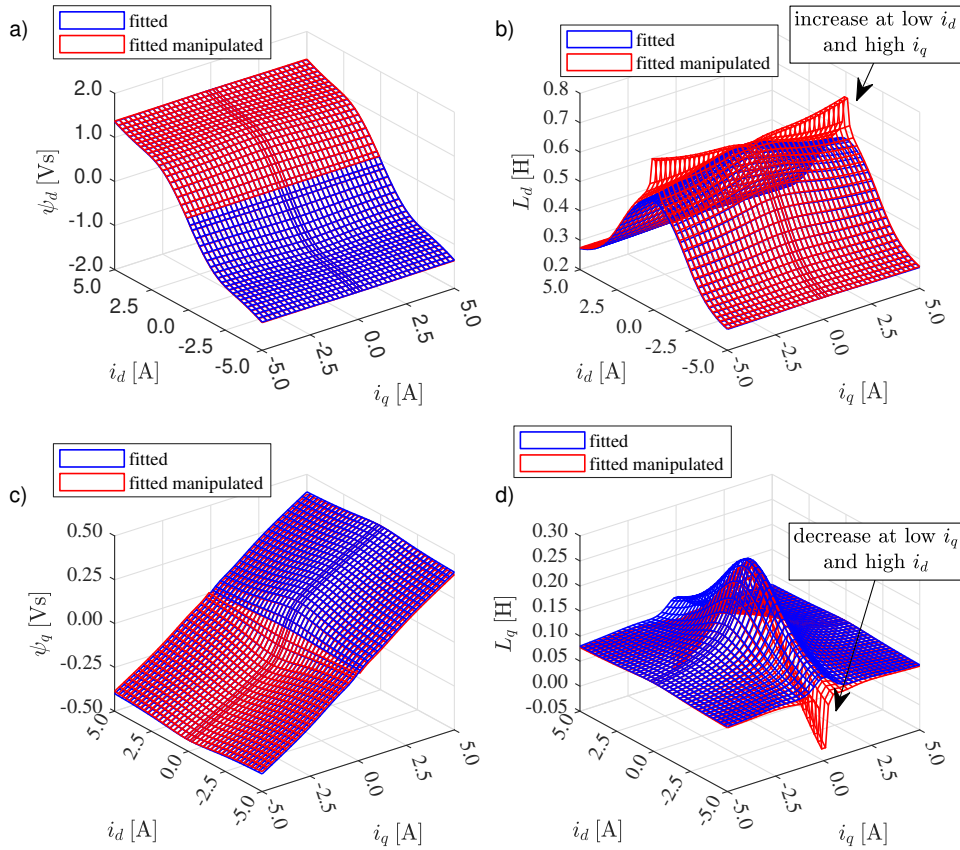


Fig. 9. The comparison of applied reference flux- and inductance model with a 4% lower resistance in the machine model (a) direct axis flux linkage, (b) direct axis static inductance, (c) quadrature axis flux linkage, (d) quadrature axis static inductance

(Fig. 7). The assumed hypothesis will be verified in the following data set. Moreover, it is assumed that the raw experimental data are not affected by the quadrature inductance component in the low current area. Thus, in this area, no corrections have to be made.

4.2. Flux and inductance surface distortion for a varying resistance error

According to the former analysis, the assumed distribution of the machine resistance was determined arbitrarily using a trial-and-error procedure based on some expert knowledge. It has been recognized that the resistance change should correspond to an exponential distribution since it is related to heating the machine windings. The assumed function was as follows:

$$\hat{R}_s = R_0 + \Delta R(1 - \exp(-i_d/\xi)), \quad (16)$$

where: \hat{R}_s , R_0 , ΔR are the estimated, initial, and deviation to the machine resistance value, and ξ is the resistance decay constant. The deviation of resistance ΔR is related to the stator heating up. The function coefficients were selected based on the manipulated simulation results to obtain the best possible match with the raw experimental data. The final resistance distribution is shown in Fig. 10.

The simulated data for the assumed resistance distribution is shown in Fig. 11. The simulated data for the manipulated

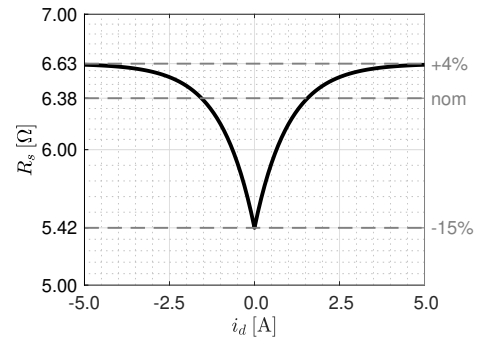


Fig. 10. The assumed resistance distribution in the machine model

model with resistance variations were compared with the fitted model (a and c) and the raw experimental data (b and d). It can be observed that the fitted model is not affected by the inductance distortions and reveals a proper self- and cross-saturation behavior. It partially matches the manipulated data, mainly in the regions where the estimation error caused by the resistance variations becomes less significant. The comparison to the raw experimental data reveals a good convergence of the distorted raw data with the manipulated model-based ones. This can be recognized as a confirmation of the distortion origin, namely the influence of resistance mismatch caused by resistance variations during the experiments. It can be indicated that the hypothesis

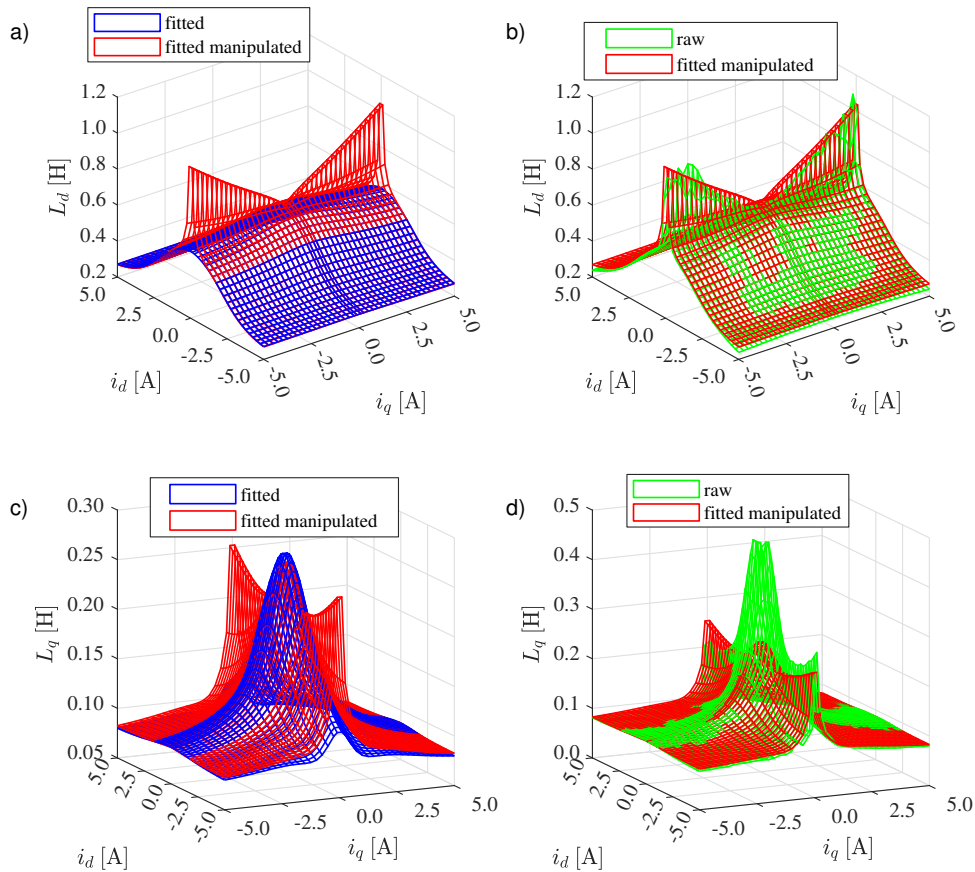


Fig. 11. The comparison of applied reference flux- and inductance model with the assumed exponential distribution of machine model resistance (a) direct axis flux linkage, (b) direct axis static inductance, (c) quadrature axis flux linkage, (d) quadrature axis static inductance

formulated by the Authors is validated, and the manipulated model reflects the raw experimental data. Thus, the observed nonphysical behavior in the raw experimental data is caused by the impact of resistance mismatch. It has to be pointed out that the applied model has not fully reflected the rapid saturation effect in the quadrature axis. This is recognized as a limitation of the applied approximation functions, which could not correctly fit into the sudden drop for the quadrature inductance component. Therefore, the functions should be revised, and an enhancement could be proposed in future developments.

5. DYNAMIC MODEL QUALITY VERIFICATION

The transient current response of the investigated motor is applied to verify the model reliability. The examination was conducted by applying motor voltage step changes in the synchronous frame while the shaft rotated at a fixed angular velocity. The test bed configuration was almost identical to the data-collecting stage, differing by the drive operating mode. The voltage components were selected and applied directly to the machine stator, and no current control unit was employed. This resulted in a freewheeling open-loop motor current response. The recorded experimental results were compared to the model-based simulational data. The current component transients caused torque variations; thus, the angular velocity varied

for short periods during the experiments. To mitigate its influence, the simulations were conducted by applying the recorded angular velocity signal in the designed model. A simulational data set was prepared for the model developed in this paper using Plexim PLECS software. The dynamic response comparison for an identified model based on deteriorated data by electrical angle misalignment and no dead-time compensation can be found in [18].

The experimental validation of the proposed mathematical model for the rising direct current component (test A) is shown in Fig. 12, and for the falling direct current component (test B) is shown in Fig. 13. It should be pointed out that the voltage transients were selected so that the trajectory of the forced current components covered as much of the drive operating range as possible. It can be seen that the transient characteristics of the developed model fit relatively well with the experimental data, the average value of the relative error does not exceed 5% (with respect to the rated current value). It can be seen that the error distribution for the direct axis is around zero – there is not any constant offset present. The error distribution indicates that the observed deviations for the d -axis are related to higher harmonic components of the measured current. An increasing offset is observed for the quadrature current component, which could be expected since the main differences between the raw data and the developed model are observed for

Ł. J. Niewiara, M. Gierczyński, T. Tarczewski, and L. M. Grzesiak

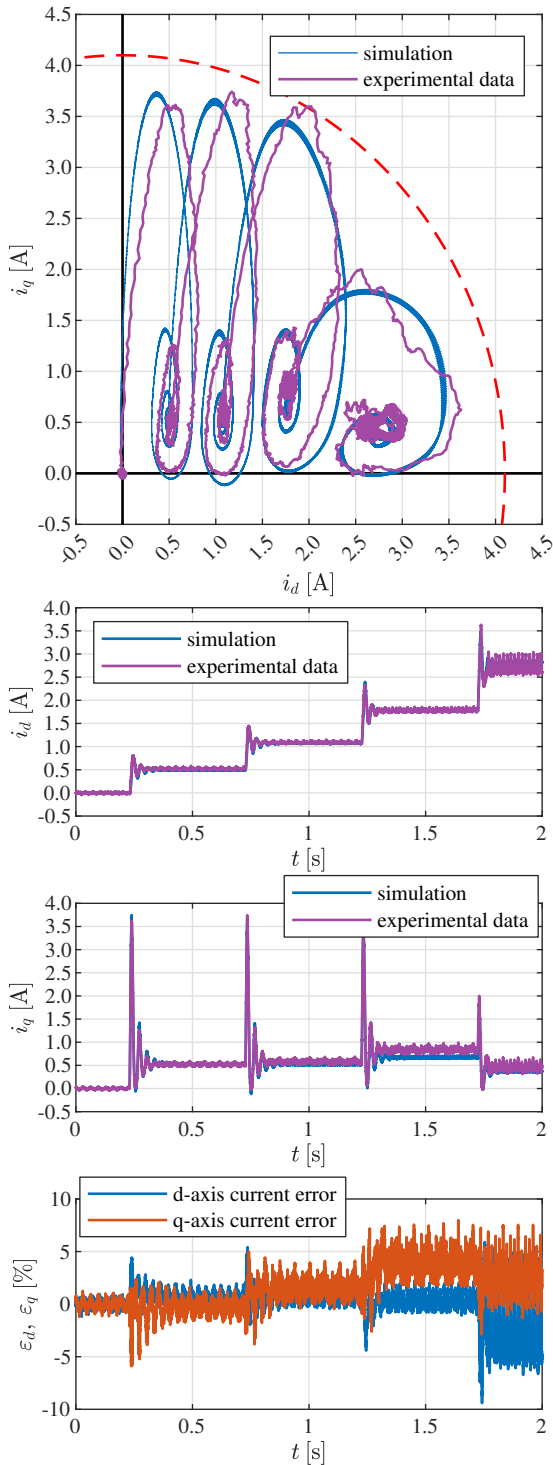


Fig. 12. Freewheeling current component trajectory and current time response for the open loop test A

the quadrature component. This results in an increasing error for the higher quadrature current components. The oscillation frequency during transients and the steady state converge with the experimental data. Some tracking error is observed in Fig. 12, but generally, the transient characteristics match well with the experimental results. It should be mentioned that the recorded data applied to the model development were partially affected

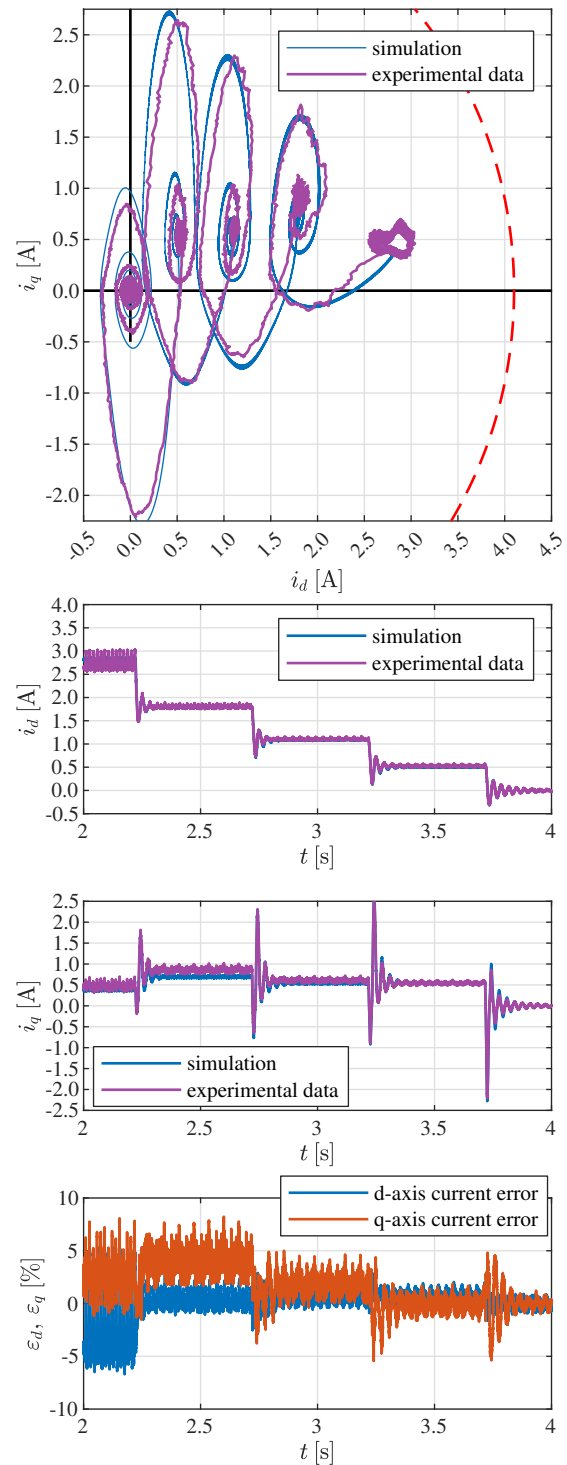


Fig. 13. Freewheeling current component trajectory and current time response for the open loop test B

by parameter uncertainties and measurement errors, and the applied model does not consider any iron losses. Moreover, the implemented model is designed for the fundamental harmonic component of the machine phase currents. Hence, higher-order harmonics in the phase currents will result in some tracking errors. Therefore, there is a tracking error caused by the model accuracy. Nevertheless, the final results are satisfying.

The developed model fits the experimental data relatively well in test B with a small and acceptable tracking error. The observed differences result from unmodeled non-linear factors in the inverter power stage, measurement errors, and parameter uncertainties of the electrical circuit (resistance variations, iron losses). Thus, the accuracy of the developed model is limited, but it is still sufficiently good to apply for modeling the investigated motor electrical circuit. The average value of the relative error does not exceed 5%. Similarly, an increasing offset value is present for the quadrature current component, which confirms that the identification procedure is more sensitive for the quadrature axis corresponding to the flux barriers distribution. Meanwhile, the direct axis is affected by an error distribution around zero without any offset observed.

It should be noted that such dynamic tests were presented for the first time by the Authors in [18]. In contrast, other authors conclude their identification results only based on the intuitive examination of the flux linkages picture and its fitness with the proposed approximation function [10, 13, 19, 21, 22]. The presented test was developed based on knowledge of the spiral shape of the current space vector trajectories during voltage steps, allowing it to cover the majority of the drive operating region with a single straightforward test. Additionally, it allows for validating the quality of the identified parameters set under relatively harsh conditions. The developed test is reliable because it

directly compares the developed model with a machine transient response. Moreover, it is relatively easy to implement since the experimental bed can already provide a running rotor test.

6. INFLUENCE OF THE ENCODER MISALIGNMENT AND LACK OF ELECTRICAL ANGLE PREDICTION

To complete the provided analysis, an additional investigation is needed to determine the impact of the position sensor misalignment and lack of electrical angle prediction for the inverse Park transformation. In this study, it is recommended that those factors be eliminated to ensure a proper configuration of the experimental setup. The performed numerical simulations provide knowledge about the impact of those factors on the raw experimental data, giving a better understanding of possible anomalies in the analyzed data.

Since the developed simulation model is assumed to be a reference one (the relative error is in an acceptable range), it is applied as a reference model to simulate the additional factors related to setup configuration. The impact of position sensor misalignment and the lack of electrical angle prediction for inverse park transformation have been simulated.

The numerical results for the position sensor offset are shown in Fig. 14. The electric angle offset was assumed for one de-

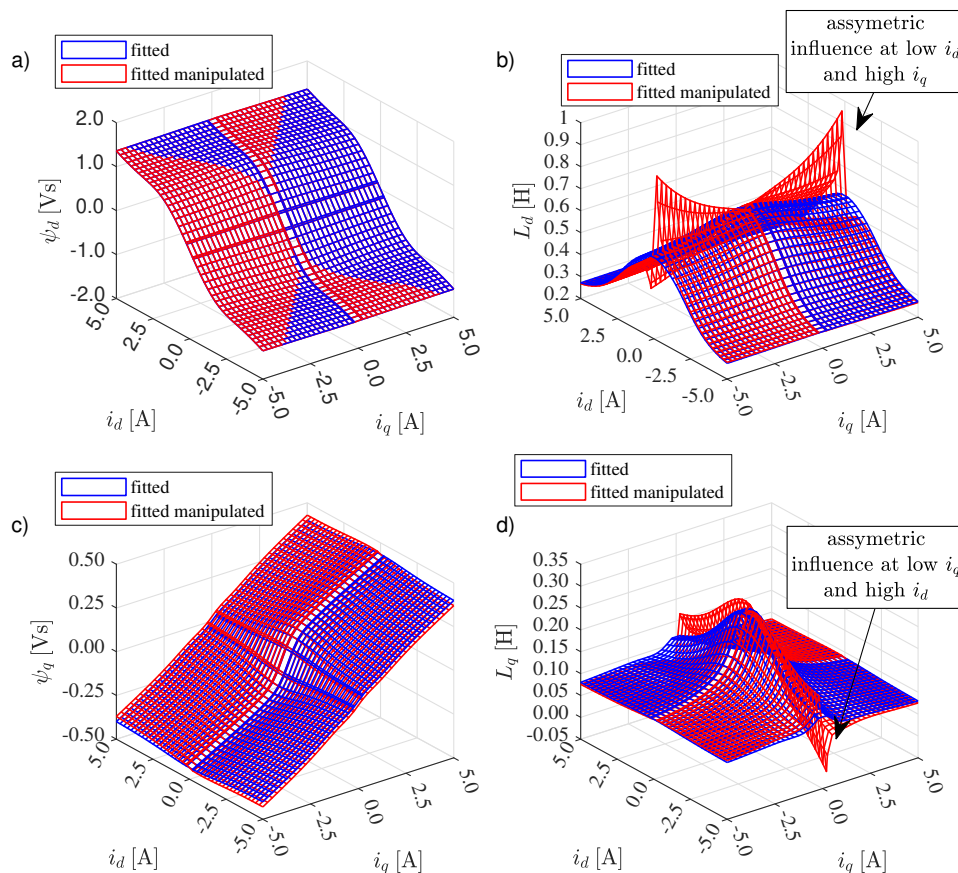


Fig. 14. The comparison of applied reference flux- and inductance model with the model obtained with simulated one electrical degree misalignment of the d-axis (a) direct axis flux linkage, (b) direct axis static inductance, (c) quadrature axis flux linkage, (d) quadrature axis static inductance

gree; its value corresponds to the angle offset, which would be present if the d -axis angle alignment was determined using only one current vector ($V1$) instead of the proposed multivector procedure. The influence of this error is mainly revealed for the inductance surfaces for low d -axis current values for the direct inductance component and low q -axis current values for the quadrature inductance component. This factor introduces an asymmetric distortion in the flux linkage and inductance component surfaces.

The anomalies observed in flux linkage distortions correspond to a surface rotation along the quadrature axis. This leads to a nonphysical flux linkage behavior, where it increases along the orthogonal current component. A similar effect has been discussed in [18] about an improperly aligned position sensor. This will not occur if the angle offset is determined using the proposed alignment procedure based on a multivector approach.

Figure 15 shows the impact of no electrical angle prediction for inverse Park transformation. Unlike the recommended configuration depicted in the provided timing diagram, the simulation model was prepared without angle prediction in the control signal transformation (Fig. 4). The impact of this error is revealed primarily in the inductance component surfaces. There is an increase in the estimated value of the direct inductance component for small values of the self-axis current and an ap-

parent decrease in the estimated value of the quadrature axis component for small values of self-axis current. This effect seems similar if the machine resistance is lower than the assumed value. Therefore, these two effects could be confused with each other, although their influence on the direct axis inductance component is different. Note that, in the absence of angle prediction, this influence does not increase as rapidly with the value of the orthogonal current component (q -axis) as in the case of incorrect resistance values. The presented identification procedure recommends the electrical angle prediction. It can be indicated that this approach allows the mitigation of this particular error source since the estimated raw experimental data (Fig. 6) does not contain a simultaneous increase of the direct axis inductance component with a sudden drop in the quadrature axis inductance component along the orthogonal current component for both of them.

The provided numerical data reveal the impact of the factors related to electrical angle issues. The observed anomalies will provide a better understanding of the possible distortions in raw experimental data related to an improper configuration of the experimental setup. The presence of the recognized anomalies may indicate a necessity for a more careful configuration of the system, according to the recommendations formulated in this study.

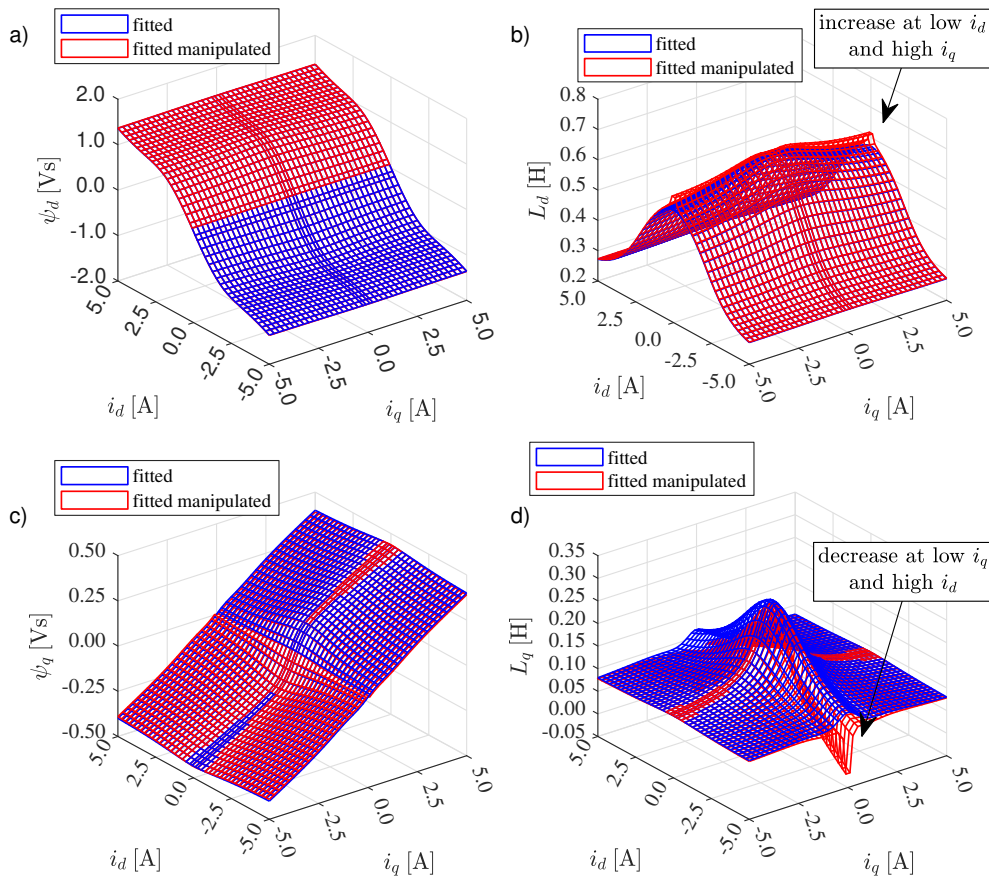


Fig. 15. The comparison of applied reference flux- and inductance model with the model obtained with simulated lack of the angle prediction for the inverse Park transformation (a) direct axis flux linkage, (b) direct axis static inductance, (c) quadrature axis flux linkage, (d) quadrature axis static inductance

7. CONCLUSIONS

The paper discusses in detail the modeling and identification approach for an RSM, particularly emphasizing the configuration of the experimental setup. The proposed model converges with the reference machine response, resulting in an acceptable error. A new approach for model evaluation has been proposed, which is simultaneously reliable and relatively simple to conduct. Moreover, the impact of several error sources on the estimated flux-linkage and inductance components surfaces is highlighted, which can help potential readers identify the issues in their raw experimental data and give a better understanding of the observed anomalies.

It was found that it is essential to use the analytical fitting function designed so that its structure assures the proper shape of the flux surfaces (according to the physical phenomena of self- and cross-saturation). If this is assured, the fitting process can partially eliminate local errors in the raw data, which are present due to some imperfections in the identification procedure. The used analytical function shape cannot fully reflect the shape of the raw data, especially the rapid rise of the q -axis inductance for low currents. Thus, further research is still needed to improve the functions of the used prototypes.

The analysis reveals that the proposed approach is vulnerable to the heating up of the winding and the rise in resistance caused by that, which, together with the long time duration, are the main limitations of the presented technique. Hence, there is a need to improve the proposed procedure to eliminate this problem.

Besides the identification procedure itself, the design of the experiment is also an essential factor influencing the results. This means that the influence of some error sources on the obtained results can depend on the sequential order of the measurement points and the period between the measurements, as it affects machine heating. This means that the sequential order of measurements should also be chosen carefully when conducting the experiments. It has been found that the recommendations for the configuration of the experimental setup will limit the risk of collecting distorted experimental data.

ACKNOWLEDGEMENTS

This research was supported by the ‘Excellence Initiative—Research University’ program of Warsaw University of Technology under grant ‘ENERGYTECH-1 Power’ and by the ‘Excellence Initiative—Research University’ program of Nicolaus Copernicus University.

REFERENCES

- [1] M. Murataliyev, M. Degano, M. Di Nardo, N. Bianchi, and C. Gerada, “Synchronous reluctance machines: A comprehensive review and technology comparison,” *Proc. IEEE*, vol. 110, no. 3, pp. 382–399, 2022.
- [2] S.-W. Su, H. Börngen, C. Hackl, and R. Kennel, “Nonlinear current control of reluctance synchronous machines with analytical flux linkage prototype functions,” *IEEE Open J. Ind. Electron. Soc.*, vol. 110, pp. 582–593, 2022.
- [3] F. Oliveira and A. Ukil, “Comparative performance analysis of induction and synchronous reluctance motors in chiller systems for energy efficient buildings,” *IEEE Trans. Ind. Inform.*, vol. 15, no. 8, pp. 4384–4393, 2019.
- [4] J.-C. Li, M. Xin, Z.-N. Fan, and R. Liu, “Design and experimental evaluation of a 12 kw large synchronous reluctance motor and control system for elevator traction,” *IEEE Access*, vol. 8, pp. 34 256–34 264, 2020.
- [5] G.V. Kumar, C.-H. Chuang, M.-Z. Lu, and C.-M. Liaw, “Development of an electric vehicle synchronous reluctance motor drive,” *IEEE Trans. Veh. Technol.*, vol. 69, no. 5, pp. 5012–5024, 2020.
- [6] A. Danilevičius, M. Karpenko, and V. Křivánek, “Research on the noise pollution from different vehicle categories in the urban area,” *Transport*, vol. 38, no. 1, pp. 1–11, 2023.
- [7] I. Boldea and L. Tutelea, *Reluctance electric machines: design and control*. CRC Press, 2018.
- [8] E. Armando, R. Bojoi, I. Radu, P. Guglielmi, G. Pellegrino, and M. Pastorelli, “Experimental identification of the magnetic model of synchronous machines,” *IEEE Trans. Ind. Appl.*, vol. 49, no. 5, pp. 2116–2125, 2013.
- [9] L. Niewiara, T. Tarczewski, and L. Grzesiak, “Angular velocity control of reluctance synchronous motor with torque maximization and gain-scheduled current controllers,” in *Proc. XVth Sci. Conf. SENE 2022*, Lodz, Poland: Lodz University of Technology, 2022.
- [10] S. Yamamoto, T. Ara, and K. Matsuse, “A method to calculate transient characteristics of synchronous reluctance motors considering iron loss and cross-magnetic saturation,” *IEEE Trans. Ind. Appl.*, vol. 43, no. 1, pp. 47–56, Jan.-Feb. 2007.
- [11] A. Credo, G. Fabri, M. Villani, and M. Popescu, “Adopting the topology optimization in the design of high-speed synchronous reluctance motors for electric vehicles,” *IEEE Trans. Ind. Appl.*, vol. 56, no. 5, p. 5429–5438, 2020.
- [12] J. Ahn, S.-B. Lim, K.-C. Kim, J. Lee, J. Choi, S. Kim, and J. Hong, “Field weakening control of synchronous reluctance motor for electric power steering,” *Electr. Power Appl., IET*, vol. 1, pp. 565–570, 2007.
- [13] A. Accetta, M. Cirrincione, M. Pucci, and A. Sferlazza, “A space-vector state dynamic model of the synchronous reluctance motor including self and cross-saturation effects and its parameters estimation,” in *2018 IEEE Energy Convers. Congr. Expo.*, Portland, USA: IEEE, 2018, pp. 4466–4472.
- [14] S. Wiedemann and C. M. Hackl, “Simultaneous identification of inverter and machine nonlinearities for self-commissioning of electrical synchronous machine drives,” *IEEE Trans. Energy Convers.*, vol. 38, no. 3, pp. 1767–1780, 2023.
- [15] S.W. Su, N. Monzen, R. Kennel, and C.M. Hackl, “Self-identification of reluctance synchronous machines with analytical flux linkage prototype functions,” in *Proc. 11th Internat. Conf. Power Electron. and ECCE Asia (ICPE 2023 – ECCE Asia)*, IEEE, 2023, pp. 221–227.
- [16] N. Monzen, B. Pfeifer, and C.M. Hackl, “A simple disturbance observer for stator flux linkage estimation of nonlinear synchronous machines,” in *32nd IEEE Int. Symp. Ind. Electron. (ISIE)*. IEEE, 2023, pp. 1–6.
- [17] A. Accetta, M. Cirrincione, M. Pucci, and A. Sferlazza, “Space-vector state dynamic model of the synrm considering self, cross-

- saturation and iron losses and related identification technique,” *IEEE Trans. Ind. Appl.*, vol. 59, no. 3, pp. 3320–3331, 2023.
- [18] Ł.J. Niewiara, M. Gierczynski, T. Tarczewski, and L.M. Grzesiak, “Practical approach for identification and dynamic modeling of reluctance synchronous motors’ electrical circuit,” in *Proc. XVIth Sci. Conf. SENE 2023*, Lodz, Poland: Lodz University of Technology, 2023.
- [19] A. Accetta, M. Cirrincione, M. Pucci, and A. Sferlazza, “A saturation model of the synchronous reluctance motor and its identification by genetic algorithms,” in *2018 IEEE Energy Convers. Congr. Expo.*, Portland, USA: IEEE, 2018, pp. 4460–4465.
- [20] Ł.J. Niewiara, T. Tarczewski, and L.M. Grzesiak, “Application of extended Kalman filter for estimation of periodic disturbance and velocity ripple reduction in pmsm drive,” *Bull. Pol. Acad. Sci. Tech. Sci.*, vol. 68, no. 5, p. 983–995, 2020.
- [21] R. Thike and P. Pillay, “Automated current control method for flux-linkage measurement of synchronous reluctance machines,” *IEEE Trans. Ind. Appl.*, vol. 56, no. 2, pp. 1464–1474, 2020.
- [22] R. Thike and P. Pillay, “Automatic inductance measurements of synchronous reluctance machines including cross-saturation using real-time systems,” in *2018 IEEE Energy Convers. Congr. Expo.*, Portland, USA: IEEE, 2018, pp. 6121–6127.